ChemPubSoc Europe

DOI: 10.1002/cctc.201700429

CHEMCATCHEM Full Papers

Iron Nanoparticles Embedded in Graphitic Carbon Matrix as Heterogeneous Catalysts for the Oxidative C–N Coupling of Aromatic N–H Compounds and Amides

Jinbao He,[a] Amarajothi Dhakshinamoorthy,*[b] Ana Primo,[a] and Hermenegildo Garcia*[a, c]

Fe or Co nanoparticles (NPs) and two nanoparticulate Fe-Co alloys having different Fe/Co atomic ratio with average particle size ranging from 10.9 to 26.5 nm embedded in turbostratic graphitic carbon matrix have been prepared by pyrolysis at 900 °C under inert atmosphere of chitosan powders containing Fe^{2+} and Co^{2+} ions in various proportions. The resulting Fe/Co NP@C samples have been evaluated as heterogeneous catalysts for the oxidative C–N coupling of amides and aromatic N–H compounds. It was observed that sequential addition of two aliquots of *tert*-butyl hydroperoxide (TBHP) in an excess of *N*,*N*-dimethylacetamide (DMA) as solvent affords the corresponding coupling product in high yields, and the most efficient catalyst was Fe NP@C. Fe NP@C is reusable and exhibits a wide scope. The catalytic activity of Fe is supported by using highly pure Fe salt and by the observation that purposely addition of Cu^{2+} impurities even plays a detrimental effect on the catalytic activity. Mechanistic studies by quenching with 2,2,6,6-tetramethylpiperidyl-1-oxyl (TEMPO) have shown that the amide radical is the key reaction intermediate, and the role of Fe NP@C is to generate the first radicals by TBHP decomposition.

Introduction

Metal nanoparticles (MNPs) are catalysts for a wide range of organic reactions including oxidations, reductions, homo- and cross couplings, and rearrangements among other transformations.[1–4] One general problem of MNPs that can limit its application in catalysis is their low stability under the reaction conditions because of the tendency of small MNPs to increase their particle size.[4] Large particle size is generally associated to exhibit low catalytic activity.[2,5,6] A general strategy to minimize particle growth is incorporation of MNPs in porous polymeric or inorganic matrices that by interaction with the particle or by confinement stabilizes its size.[7–10] Besides the stabilization of particle-size distribution, the matrix can assist the catalytic reaction by adsorption or preactivation of the substrates; it is commonly observed that the nature and structure of the matrix exerts a strong influence on the intrinsic activity of these MNPs.[11–13]

It has been recently reported that MNPs and metal oxides obtained by pyrolysis of metal complexes can exhibit a unique catalytic activity thanks to the favorable influence of the carbonaceous matrix surrounding the MNPs, which was formed in the process.[14,15] Similarly, MNPs and metal oxides wrapped with carbon have been obtained by pyrolysis of metal organic frameworks.[16–21] Although active carbons and other types of carbons are among the preferred supports of MNPs,[22–24] the carbon-wrapped MNPs reported herein stand out by their pyrolytic formation procedure, the type of carbon that surrounds the MNPs, and the unique activity and stability of MNPs that can be achieved.

Other aspect to be considered is the nature of the metal. Although NPs of noble metals are widely used as catalysts, the interest in exploiting the potential of abundant, base metals as catalysts is increasing with regard to sustainability and affordability.[25,26] In this context, Fe, the most abundant metal, has been under the spotlight because of its ability to promote organic reactions and couplings in particular.[26,27]

Herein, a general procedure to prepare MNPs embedded in a graphitic carbon matrix (denoted as MNP@C) from natural biopolymers is presented and used to obtain a series of carbon-wrapped Fe, Co, and Fe–Co alloys. The catalytic activity of these MNP@C samples for the oxidative C–N cross coupling of aromatic N–H compounds and amides has been determined and details of the reaction mechanism involving radicals unveiled. Related precedents have reported the oxidative C–N coupling of aromatic N–H compounds with amides using di-*tert*-butyl peroxide as oxidizing agent and homogeneous Fe^{2+} catalysts[28,29] as well as a Cu metal organic framework as heterogeneous catalyst.[30] However, MNPs wrapped in graphitic

[a] J. He, Dr. A. Primo, Prof. Dr. H. Garcia
Instituto Universitario de Tecnología Química CSIC-UPV
Universitat Politècnica de València
Av. De los Naranjos s/n, 46022, Valencia (Spain)
E-mail: hgarcia@qim.upv.es

[b] Prof. Dr. A. Dhakshinamoorthy
School of Chemistry
Madurai Kamaraj University
Tamil Nadu, 625 021 (India)
E-mail: admguru@gmail.com

[c] Prof. Dr. H. Garcia
Centre of Excellence for Advanced Materials Research
King Abdulaziz University, Jeddah (Saudi Arabia)

Supporting information and the ORCID identification number(s) for the author(s) of this article can be found under https://doi.org/10.1002/cctc.201700429.

carbon, which are currently under intense investigation because of their unique catalytic activity that has frequently been observed,[31–34] have not yet been reported as catalysts for this reaction.

Results and Discussion

Catalyst preparation

Preparation of MNP@C was performed by pyrolyzing powdered samples of chitosan-containing adsorbed Fe^{2+} or Co^{2+} metal ions or the corresponding Fe^{2+}–Co^{2+} mixture at 900 °C under inert atmosphere. The chitosan samples containing Fe^{2+}/Co^{2+} metal ions were obtained by water evaporation of acid aqueous solutions of chitosan to which the appropriate amounts of the corresponding transition-metal ions (5 wt% of metal ion with respect to dry chitosan weight) were added. The preparation procedure is illustrated in Scheme 1. It has

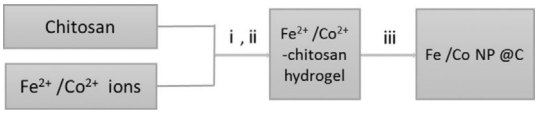

Scheme 1. Steps in the preparation of the MNP@C samples: (i) dissolution in acetic acid aqueous solutions; (ii) water evaporation; (iii) pyrolysis at 900 °C under Ar flow.

been shown in a series of studies that pyrolysis of chitosan under inert atmosphere produces a N-doped turbostratic graphitic carbon residue with some residual oxygen content (about 8 wt.%) that can be easily exfoliated by sonication.[35,36] If these samples contain metals, they can spontaneously segregate in a different phase and are simultaneously reduced to their metallic state by the so-called carbochemical reduction.[37] Upon heating a mixture of metal oxide and carbon at high temperature, the oxide becomes reduced to metal and the carbon becomes oxidized to CO_2.[38] The same behavior was expected to occur in the pyrolysis of Fe^{2+}/Co^{2+}-containing chitosan samples, resulting in the formation of MNP@C. Herein, a series of four MNP@C samples were prepared, and their elemental compositions according to chemical analysis are presented in Table 1. The "*x*" in Fe–Co_xNP@C denotes the Fe/Co atomic ratio.

Besides chemical analysis, the samples obtained according to Scheme 1 were characterized by their XRD patterns, Raman spectroscopy, and electron microscopy. XRD patterns of three selected MNP@C samples are shown in Figure 1. From the XRD

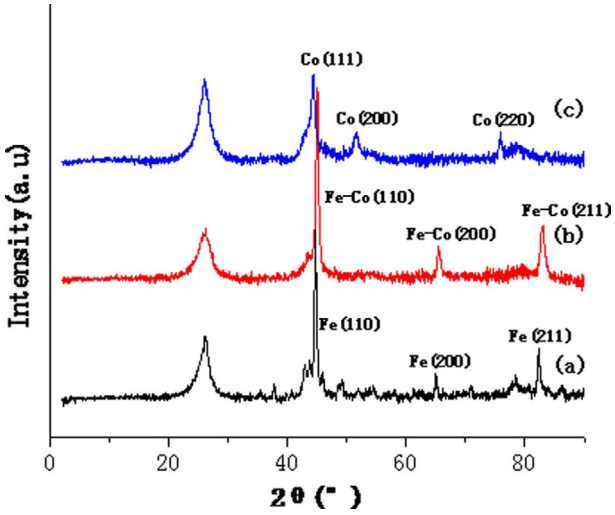

Figure 1. XRD patterns of the MNP@C prepared according to Scheme 1: (a) FeNP@C; (b) Fe–$Co_{1.42}$NP@C; (c) CoNP@C. The broad peak at $2\theta = 27°$ corresponds to the graphitic carbon residue and some weak peaks in plot (a) could indicate the presence of some Fe_3C (see text).

patterns, the presence of a significant proportion of the corresponding metal carbides or metal oxides was ruled out because the corresponding diffraction peaks were either absent of had very low intensity. Particularly for FeNP@C, weak diffraction peaks at $2\theta = 37°$ (112) and 39° (200) were recorded that are compatible with the presence of cementite (Fe_3C),[39] but their intensity was very low. In contrast, those peaks indicating the presence of Fe or Co metals were very intense. For the mixtures of Fe and Co, the minor variation in the position of the diffraction peaks at $2\theta \approx 44°$ supports the assumption that the NPs are real Fe–Co alloys, rather than independent Fe and CoNPs. By using the Scherrer equation, the average sizes of MNPs of the four samples were estimated to be 26.5, 16.3, 17.0, 10.9 nm for FeNP@C, Fe–$Co_{1.42}$NP@C, Fe-$Co_{0.86}$NP@C, CoNP@C, respectively, which agree well with the statistical average particle sizes obtained from TEM measurements. It should be commented that although no changes were observed in the XRD patterns after sample preparation and storage of the solids in vials at the ambient atmosphere, it is very likely that the outermost external part of the metal surface can become partially oxidized.

The nature of carbon residue derived from chitosan was determined by Raman spectroscopy. The Raman spectrum for FeNP@C is shown in Figure 2a. Very similar Raman spectra to those previously reported ones for turbostratic graphitic carbons lacking any metal were recorded for all the samples.[36] Thus, the expected G and D bands appearing at 1596 and 1354 cm^{-1}, respectively, were recorded together with two 2D defined peaks at 2940 and 2686 cm^{-1}. This is in accordance with the presence in the graphene sheet of defects from carbon vacancies, holes, and the residual N atoms from chitosan.[36] A quantitative indicator of the defect level of graphenic

Table 1. Chemical analysis of the MNP@C samples. The percentage of metals was determined by ICP analysis and the percentage of N, C, H was determined by combustion analysis. All values are in wt.%, and it is assumed that the difference to 100% owes to the O content.

Sample	N	C	H	Fe	Co
FeNP@C	0.98	89.76	0.14	1.02	–
Fe-$Co_{1.42}$NP@C	0.97	85.23	0.16	0.37	0.26
Fe-$Co_{0.86}$NP@C	1.04	86.02	0.16	0.62	0.72
CoNP@C	1.36	87.50	0.17	–	0.61

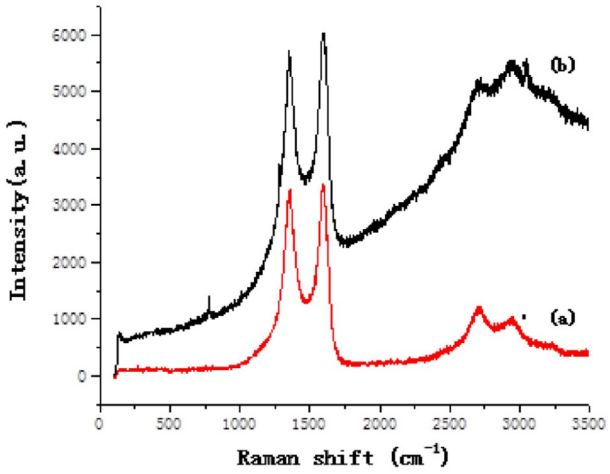

Figure 2. Raman spectra of (a) fresh and (b) recovered Fe NP@C catalyst after the C–N coupling reaction.

sheets can be given by determining the relative intensity of G and D band (I_G/I_D), which, in the present case, was 1.26 for the four MNP@C samples, corresponding to a defective, doped G. Interestingly, no vibration peaks attributable to the presence of metal oxides that should appear at low wavenumber values were observed for any of the MNP@C samples before their use as catalyst, in good agreement with the XRD patterns in which no oxides are detectable. In contrast, the recovered Fe NP@C catalyst after the C–N coupling between benzimidazole (**1 a**) and *N*,*N*-dimethylacetamide (DMA) showed the presence of iron oxide indicating that the oxidation by *tert*-butyl hydroperoxide (TBHP) takes place under the experimental conditions (Figure 2 b).

To prove the accessibility to Fe and Co NPs even if they are embedded within the graphitic carbon matrix, the Fe NP@C and Co NP@C samples were treated with an aqueous solution of diluted HCl, and it was observed that a portion of 80 to 90% of the initial metal content becomes dissolved under these conditions (see Experimental Section). This proves that the surfaces of Fe and Co metals are accessible to interact with TBHP and reagents despite their embedment in a carbon matrix.

The presence of MNPs embedded in a carbonaceous matrix was confirmed by TEM imaging of the MNP@C samples. A set of images illustrating the structure and morphology of the Fe NP@C samples are shown in Figure 3, and images of other samples are presented in the Supporting Information, Figures S.1–S.3. In dark field that also allows the estimation of the particle size distribution, MNPs were clearly distinguished. From these images, it was clear that the MNP size was not homogeneous and that there was a broad dispersion of sizes below 50 nm. However, the corresponding histogram of particle sizes counting a statistically relevant number of particles shows that particles of sizes between 5 and 10 nm are the most abundant in the MNP@C samples.

Elemental mapping of Fe and Co reveals that the locations of these two elements coincide (see Figure S5 in Supporting Information), thus confirming the XRD results that the MNPs are real Fe–Co alloys.

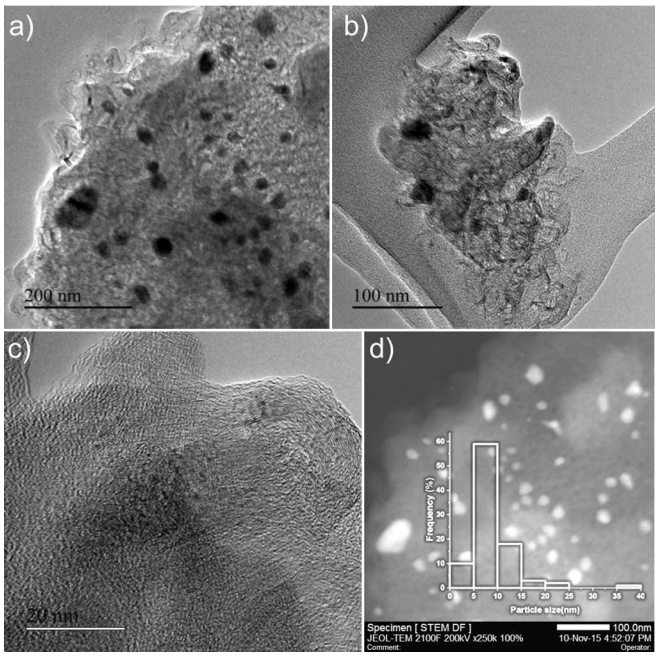

Figure 3. TEM images of Fe NP@C samples at (a,b) low (scale bar 200 nm and 100 nm, respectively) and (c) high magnification (scale bar 20 nm). (d) Dark-field image, the inset shows the statistical particle-size distribution of Fe NPs (scale bar 100 nm).

The small particle size is remarkable if considering the high temperature (900 °C) to which the MNP@C samples are submitted during the preparation procedure and the time taken in the pyrolysis (6 h). In one of the most common procedures, Fe NPs of small particle size similar to those obtained herein were obtained by chemical reduction using reverse phase emulsions employing oleylamine–water emulsions.[40] In this regard, although particles of much larger size are also detected, the present procedure allows obtaining in a single step Fe/Co NPs of small diameters and the carbon matrix in which the NPs are embedded. It is suggested that, as claimed previously, chitosan and the carbonaceous residues derived therefrom during the different phases of the pyrolysis are thwarting and restricting the growth of the Fe/Co NPs by interacting with them.[41] In related precedents, it has been found that Au,[42,43] Cu,[41] and even TiO_2[44] and CeO_2[45] NPs of relatively small size are formed if the procedure starts with the corresponding metal ions embedded in chitosan.

The composition of the uppermost part of the Fe NP@C catalyst was also characterized by X-ray photoelectron spectroscopy (XPS), and the observed peaks as well as the best fitting to individual components are given in Figure 4. The deconvoluted C 1s spectrum (Figure 4, left) can be fitted to three main peaks at 283.0, 284.5, and 288.5 eV that can be assigned to C at defects, graphenic C atoms, and sp^3 C atoms bonded to oxygen, respectively. Furthermore, analysis of the Fe 2p spectrum (Figure 4, right) reveals the existence of Fe^{2+} and Fe^{3+} at the binding energies of 709 and 711 eV, respectively. The presence of $Fe^{2+/3+}$ on the outermost part of Fe NPs is relevant from a catalytic point of view and complements the information by XRD that indicates that the predominant oxidation state of Fe

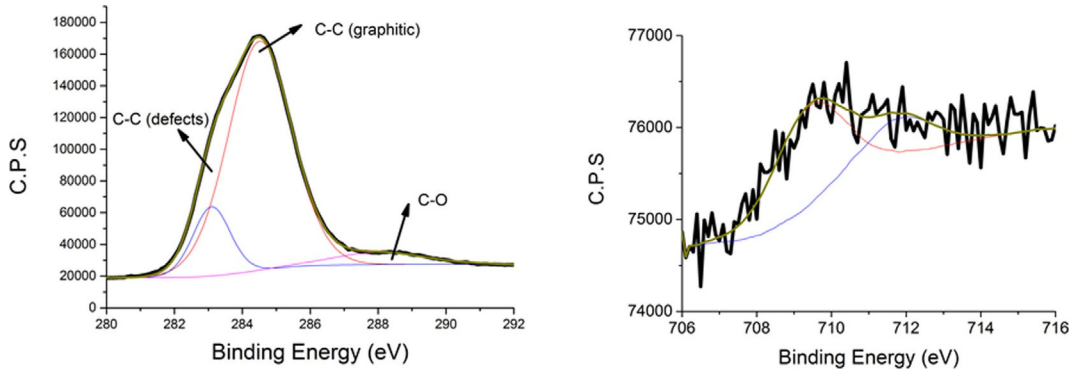

Figure 4. C 1s (left) and Fe 2p (right) peaks of the high-resolution XPS of Fe NP@C.

is Fe^0. Notably, XPS analysis probes the composition of the outermost surface of the NPs, whereas XRD probes the whole sample.

Oxidative C–N coupling

The purpose of the present study was to evaluate the catalytic activity of the Fe/Co NP@C samples as heterogeneous catalysts for the oxidative C–N coupling. Oxidative C–N couplings have the advantages that they do not require halide derivatives as substrates. Preliminary catalytic screenings were performed by using Fe NP@C as a catalyst, optimizing the amount of TBHP, the solvent, and the temperature for the coupling of **1a** and DMA. The reaction is indicated in Scheme 2. Initially, 1,2-dichloroethane (DCE) was used as a solvent because literature data suggested that this could be one of the most suitable solvents for the reaction.[28] However, in contrast to the report in the literature,[28] under our reaction conditions the C–N coupling product (**3a**) was observed as a primary, but instable product, undergoing a subsequent conversion to *N*-(2-chloroethyl)benzimidazole (**3b**) as final and stable product. A time–conversion plot of the catalytic oxidative C–N coupling using DCE as a solvent is shown in Figure 5. The product **3b** clearly derives from the reaction of **1a** with the solvent. Thus, to avoid the decomposition of **3a**, the reaction was attempted in other solvents. It was observed, however, that the reaction completely failed using *tert*-butanol, toluene, acetonitrile, or ethyl acetate as solvents.

In contrast to the negative results in some solvents, C–N coupling between **1a** and DMA could be also observed by using an excess of DMA that was acting under these conditions as reagent and solvent. In DMA, however, although the selectivity to **3a** was almost complete, conversion of **1a** was unsatisfactorily low, approximately 35%. The temporal evolution of the formation of **3a** under these conditions is shown in Figure 6.

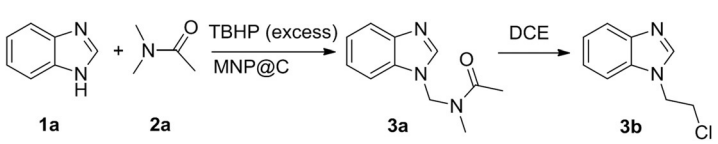

Scheme 2. Oxidative C–N coupling of benzimidazole and DMA promoted by TBHP and Fe NP@C.

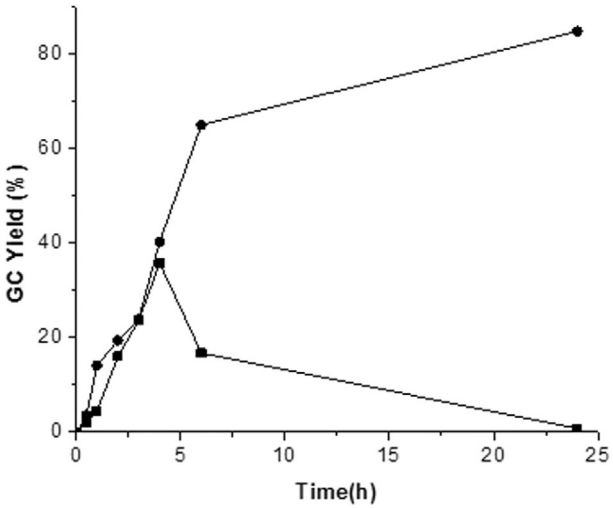

Figure 5. Time–yield plots determined by GC for the oxidative C–N coupling promoted by Fe NP@C in DCE solvent: (■) **3a**; (●) **3b**. Reaction conditions: **1a** (0.1 mmol), Fe NP@C (1.6 mol%), 2.5 equiv. oxidant (5 M solution of TBHP in decane), DCE (2 mL), Ar (2.5 bar), 110 °C.

A reason for the low yield of **3a** could be the spurious decomposition of TBHP without promoting C–N coupling. This possibility was confirmed by performing an additional experiment in which the oxidative C–N coupling reaction was initially started under the normal conditions, but as soon as the reaction rate decreased considerably, at approximately 4 h reaction time, 1.5 equivalents of TBHP were added (see Figure 6). Upon addition of the second amount of TBHP, a significant increase in the yield of **3a** from approximately 30 to 50% was quickly achieved, reaching a final **3a** yield of 65% at 20 h. Interestingly, under the present experimental conditions, no other product besides **3a** was observed and unreacted starting material **1a** was also recovered at final reaction time. Thus, the incomplete yield probably results from the spurious decomposition of TBHP.

Considering the chemical structure of DMA and its reactivity through a N-methyl substituent, a structurally related solvent that could also be suitable to over-

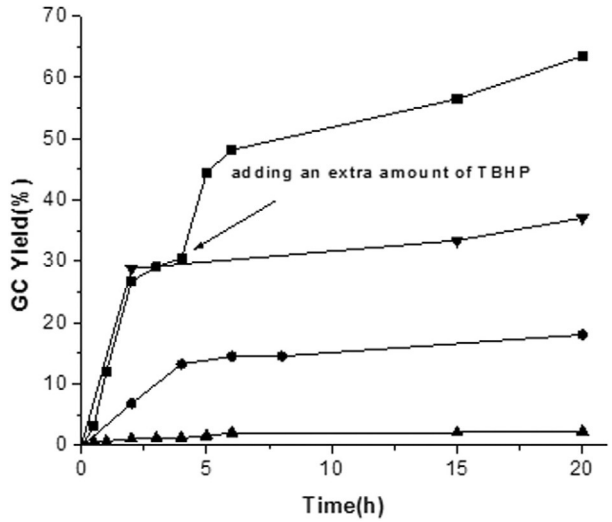

Figure 6. Time-yield plots determined by GC for two twin coupling reactions using the same reaction conditions; (■) with adding an extra amount of TBHP (1.5 equiv. TBHP from a 5 M solution of TBHP in decane) after 4 h reaction time; (▼) no adding; control experiment (▲) without any catalyst; (●) with deactivated catalyst obtained by boiling Fe NP@C in acetamide before use. Reaction conditions: **1 a** (0.1 mmol), Fe NP@C (1.6 mol%), DMA (2 mL), Ar (2.5 bar), 110 °C, 2.5 (or 4.0) eq. of TBHP from a 5 M TBHP solution in decane.

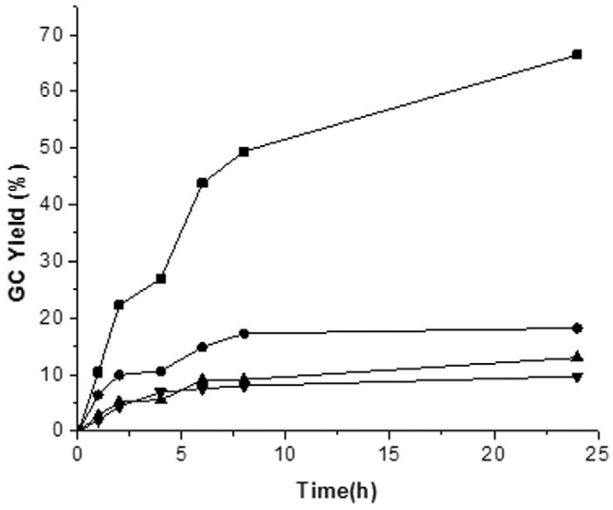

Figure 7. Time-yield plots determined by GC for the oxidative C–N coupling of **1 a** and DMA in the presence of a series of catalysts: (■) Fe NP@C; (●) $Fe–Co_{1.42}$ NP@C; (▲) $Fe–Co_{0.86}$ NP@C; (▼) Co NP@C. Reaction conditions: **1 a** (0.1 mmol), catalyst (1.6 mol%), two consecutive additions of 2.5 and 1.5 equiv. of TBHP (5 M solution in decane), DMA (2 mL), Ar (2.5 bar), 110 °C.

come the limitation of other solvents would be acetamide. Surprisingly, no **1 a** conversion was observed by using acetamide. Titration of TBHP after 24 h reaction time indicates that only a residual percentage of 11% of the initial TBHP remains, even though no **3 a** was formed. A reason for this could be that acetamide acts as a poison of Fe NP@C catalyst by strong hydrogen bonding of acetamide to the metal surface. This possibility was checked by performing an experiment in which Fe NP@C was boiled first in acetamide at 110 °C for 4 h, then it was recovered, washed with DMA, and used as catalyst in DMA as solvent. It was observed that the catalytic activity of acetamide-treated Fe NP@C was much lower than that of the fresh untreated sample (see Figure 6). This decrease in catalytic activity after contacting with acetamide suggests that the material becomes deactivated by this solvent, thus, providing some hints to rationalize the negative results observed in acetamide, in spite of its similarity with DMA.

After having found that an excess of DMA is a suitable medium to perform the oxidative coupling and optimized reaction conditions, the influence on the catalytic performance of the percentage of Co on the Fe/Co NP@C catalyst was checked by performing a series of reactions under the same conditions, but using the other MNP@C catalysts of the series. As shown in Figure 7, the presence of Co in the catalyst is detrimental for the activity that undergoes a gradual decrease as the percentage of Co increases.

To gain insight into the heterogeneity of the MNP@C-catalyzed reaction, the solid catalysts were removed by filtration after 24 h reaction, and the clear solutions were analyzed by inductively coupled plasma optical emission spectroscopy (ICP–OES). Irrespective of the MNP@C material used, the Fe amount leached to the solution was 0.72 μg, whereas, for instance, the initial Fe amount of the Fe NP@C (1.6 mol%) with a Fe loading of 1.02 wt% was 93 μg. Thus, more than 99.2% of the Fe initially present was retained in the catalyst. It was, however, observed that filtration of the Fe NP@C catalyst did not completely stops the reaction. Once initiated the reaction, formation of C–N coupling products also occurred even after filtration of the Fe NP@C catalyst at 4 h, although in approximately 40% lower percentage than without filtration of the catalyst. This formation of product **3 a** in the absence of catalyst is proposed to be related to the reaction mechanism involving C-centered radicals as reaction intermediates and the role of Fe NP@C as radical initiator as discussed below.

To learn more about the role of leached Fe species as a homogeneous catalyst, three control experiments using soluble precursors with Fe in different initial oxidation states were performed. Specifically, the compounds used were $Fe(CO)_5$, $FeCl_2$, and $Fe(OAc)_3$, with Fe in 0, +2, and +3 oxidation state, respectively. The amount of these materials used was such as to provide a weight of Fe approximately twice (1.5 μg) as determined by ICP at the final reaction time. It was, however, observed that although compound **3 a** was detected at final reaction time, the percentage of C–N coupling was in all cases below 5%, indicating that the contribution of the leached Fe to the observed yield of **3 a** is negligible.

Reusability and catalyst stability

Reusability and catalyst stability are important issues in heterogeneous catalysis and have to be addressed. Aimed at determining catalyst stability, the same Fe NP@C sample was submitted to a series of consecutive uses under the optimal reaction conditions. As shown in Figure 8, a gradual decrease in the catalytic activity was observed. Careful perusal of the time-conversion plots indicate, however, that the decay in the cata-

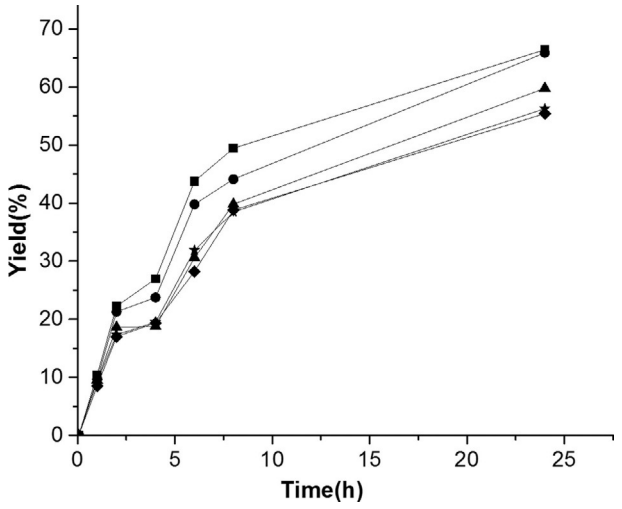

Figure 8. Time–yield plots determined by GC for the reusability test of the catalyst: (■) first use; (●) second use; (▲) third use; (★) fourth use; (◆) fifth use. Reaction conditions: **1a** (0.1 mmol), Fe NP@C (1.6 mol%), two consecutive additions of 2.5 and 1.5 equiv. of TBHP (5 M solution in decane), DMA (2 mL), Ar (2.5 bar), 110 °C.

lytic activity is mainly caused by the lower **3a** yield achieved in the first TBHP addition (see data points at times shorter than 4 h in Figure 8), and the profile corresponding to the second addition is very similar with no decay in the reaction rates for five reuses. Thus, the decay observed in the yield at final reaction time seems to be owing to the operation of a very fast spurious decomposition of TBHP occurring for the used Fe NP@C sample at the initial stages of the recycling and/or some unavoidable loss of catalyst mass during reuse. It seems, however, that after this variation at initial times, the time–conversion plots are parallel upon reuse, indicating that the reaction rates for the oxidative C–N coupling do not change upon reuse and that the activity of Fe NP@C sample remains constant besides the spurious TBHP decomposition. It could be that this fast TBHP decomposition is an artifact caused by the recycling procedure.

Furthermore, the Fe NP@C sample resulting after five consecutive reuses was again imaged by TEM trying to determine variations of Fe particle size. It was, however, determined that the average Fe particle size did not undergo clear variation upon use of the sample as catalyst. In addition, also the morphology of the C matrix remained unaltered. Images of one of the used samples are presented in Figure 9, together with the corresponding particle size histogram.

Role of Cu impurities

An additional point of concern using Fe as catalyst is the role of impurities on the observed catalytic activity. It should be noted that the samples in the present study were prepared by using a Fe salt precursor with a nominal purity of 99.99% and, therefore, the maximum expected proportion of metal impurities should be below 100 ppm. Considering the precedents that have shown that Cu is the most common Fe impurity that

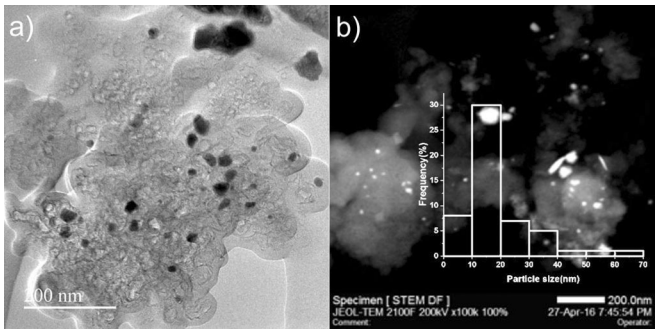

Figure 9. TEM images of five -times-used Fe NP@C under (a) bright and (b) dark field. The inset shows the particle-size distribution of this used Fe NP@C sample. Scale bars 200 nm.

could contribute to the apparent catalytic activity of Fe in other cross-coupling reactions,[27,46] the influence of the presence of Cu on the catalytic activity of Fe NP@C was investigated by preparing two additional Fe NP@C samples purposely containing 10 and 20 ppm of Cu. The results are presented in Figure 10. The presence of Cu even in minute amounts has a detrimental influence, decreasing the initial reaction rate of Fe NP@C from 1.23 mmol g^{-1} h^{-1} to 0.98 mmol g^{-1} h^{-1}, and the yield at final time from 66.4% to 64.3%. Extrapolation at 0 ppm of Cu content of the plot of the initial reaction rate against the level of Cu impurity strongly supports that Fe has intrinsic catalytic activity for the oxidative C–N coupling.

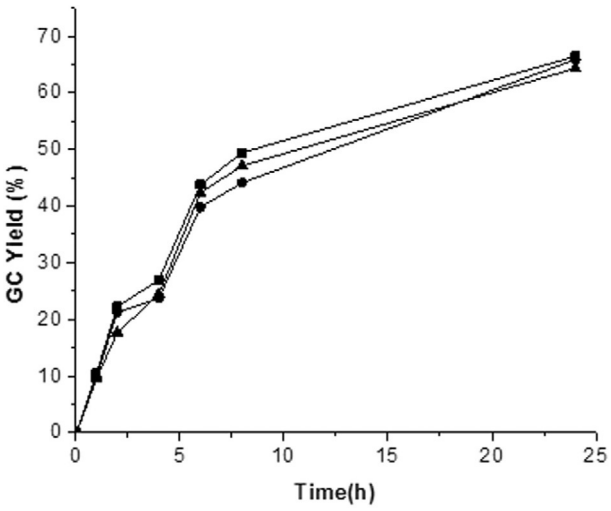

Figure 10. Time-yield plots determined by GC for the oxidative C–N coupling with Fe salt precursor containing two different proportions of Cu impurities: (■) Fe salt precursor with a purity of 99.99%; (▲) Fe salt precursor with a purity of 99.99% contaminated with 10 ppm of Cu; (●) Fe salt precursor with a purity of 99.99% contaminated with 20 ppm of Cu. Reaction conditions: **1a** (0.1 mmol), Fe NP@C (1.6 mol%), two consecutive additions of 2.5 and 1.5 equiv of TBHP (5 M solution in decane), DMA (2 mL), Ar (2.5 bar), 110 °C.

Reaction mechanism

The reaction mechanism of the oxidative C–N coupling, even in homogeneous phase, has not been yet disclosed.[28] To gain

insight on the reaction mechanism, a series of control experiments were performed in the presence of 2,2,6,6-tetramethylpiperidyl-1-oxyl (TEMPO) as a quencher of possible C-centered radical intermediates. In this way, the reaction of DMA with **1a** using Fe NP@C as the catalyst in the presence of TEMPO did not afford the expected product **3a** (Scheme 3). In contrast, adducts between DMA with TEMPO (**A**) and the C–N coupling product with TEMPO (**B**) were observed from the analysis of the reaction mixture by GC–MS. On the other hand, a similar control experiment of DMA, TBHP, and TEMPO in the absence of **1a** resulted exclusively in the formation of adduct **A** between DMA and TEMPO. These experiments strongly support that the reaction proceeds through the formation of the radical from DMA.

Furthermore, if the adduct of DMA and TEMPO is first generated by TBHP in the presence of Fe NP@C, and, then, the Fe NP@C is removed, **1a** is added and the mixture heated at 140 °C, formation of the C–N coupling product **3a** was observed concomitantly with the disappearance of the DMA-TEMPO adduct **A**. This experiment is interpreted considering that the DMA–TEMPO adduct is acting as a dormant radical of DMA, because upon heating, it would reversibly release some DMA radical. This DMA radical would couple with **1a** without the need of any catalyst. In this way, the role of Fe NP@C catalyst would be merely to act as initiator decomposing TBHP, generating the first radicals that would form C-centered DMA radicals. As the homogeneous catalysts reported for this reaction are $Fe(OAc)_2$ and $FeCl_2$, and the XPS results reveal that the surface of Fe NPs has a +2 and +3 oxidation state, it is probably that these surface species act similarly to the homogeneous counterparts coordinating to TBHP and, then, splitting the reagent in the initial oxygen-centered radicals (Scheme 3). This role of Fe generating radicals and the intermediacy of radicals is compatible with the observation indicated above that filtration of Fe NP@C does not completely stops the reaction. As radical reactions occur through radical chain mechanism, depending on the length of the propagation steps, some product formation can be observed even upon removal of the initiator, although the initiator can generate new radicals at any reaction time.

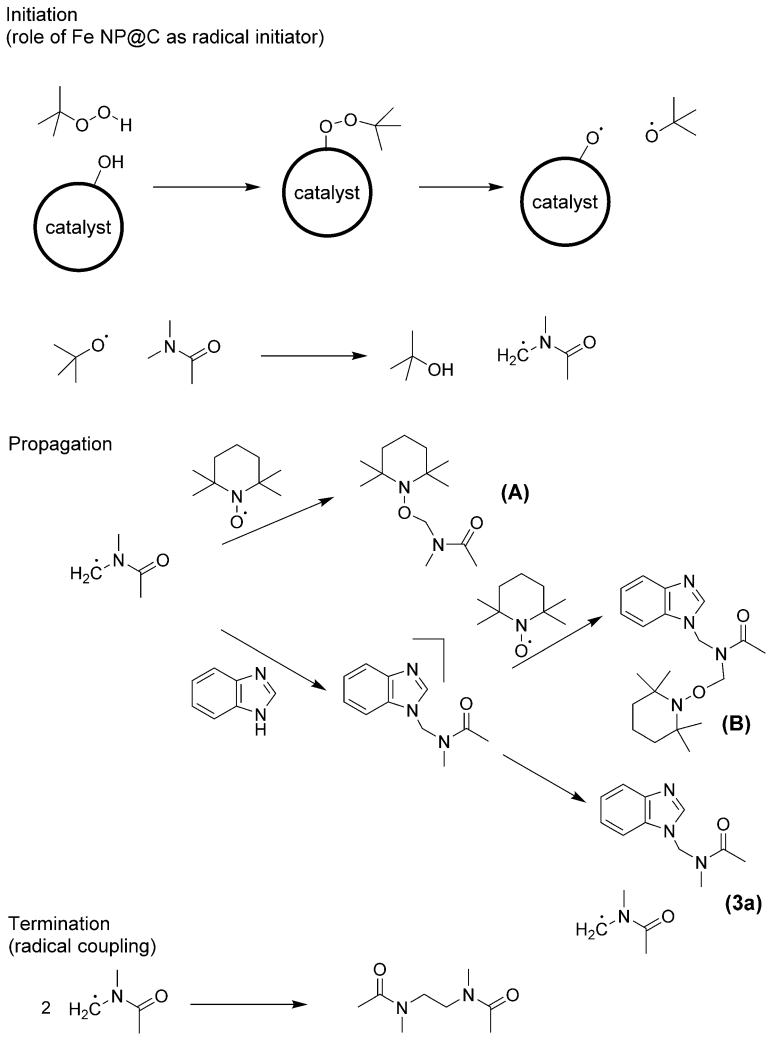

Scheme 3. Possible reaction mechanism, role of Fe NP@C catalyst, and quenching of intermediates by TEMPO.

Scope of the reaction

Finally, the scope of the reaction was screened by using Fe NP@C as a catalyst to promote the oxidative C–N coupling of amides with other N–H substrates. The results are presented in Table 2. High to moderate yields were obtained in all cases, except in the case of 2-phenylbenzimidazole, for which low yields were attained. It seems that for 2-phenybenzimidazole, steric encumbrance attributable to the presence of a 2-phenyl substituent at the neighbor position makes C–N coupling more difficult. In contrast, 2-methylbenzimidazole affords the expected C–N coupling product in even higher yields than **1a**. Similar increase in the yield of the coupling product is observed comparing the results obtained with pyrazole and 3,5-dimethylpyrazole. Besides using DMA, the scope of the oxidative C–N coupling was also expanded by using two other amides, namely, ε-caprolactam and γ-butyrolactam, reaching good to moderate yields under the general reaction conditions.

Table 2. Products formed in the oxidative C–N coupling of DMA with N–H substrates catalyzed by Fe NP@C.[a]

Product yields[b]

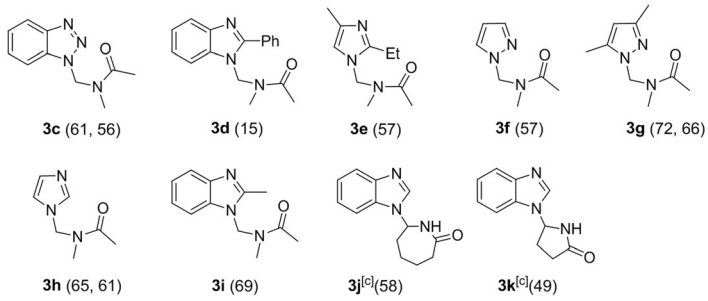

3c (61, 56) **3d** (15) **3e** (57) **3f** (57) **3g** (72, 66)

3h (65, 61) **3i** (69) **3j**[c](58) **3k**[c](49)

[a] Reaction conditions: N compound (0.1 mmol), Fe NP@C (1.6 mol%), two consecutive additions of 2.5 and 1.5 equiv. of TBHP (5 M solution in decane), DMA (2 mL), Ar (2.5 bar), 110 °C, 24 h; [b] the numbers in brackets correspond to the values determined by GC and if there is a second value, it corresponds to the isolated yield; [c] the reaction was performed with 5 mol% of Fe NP@C.

Conclusions

It is shown that chitosan-containing first-row transition metal ions, Fe^{2+} and Co^{2+}, are suitable precursors to form metal nanoparticles (MNPs), either of a single metal or as nanoparticle alloys, embedded within graphitic carbon matrix. The resulting carbonaceous MNP@C composites can be suitable materials to be used as heterogeneous catalysts. Their catalytic activity has been evaluated for the oxidative C–N coupling, and a large influence of the nature of the metal catalyst and the solvent has been found. In spite of the apparent decrease in catalytic activity, Fe NP@C appears as a stable catalyst for the process with a broad scope. The reaction mechanism involves the generation of amide radicals by decomposition of TBHP promoted by the Fe NP@C catalyst.

Experimental Section

Reagents

Commercially available reagents and solvents were purchased from Aldrich and used without further purification, except chitosan that was purified by filtration of acid aqueous solutions.

Synthesis of MNP@C

Briefly, Fe-$Co_{1.42}$ NP@C, Fe-$Co_{0.86}$ NP@C were prepared by mixing chitosan (400 mg) in a 20 mL aqueous solution of $Fe(OAc)_2$ (20.5 mg) and $Co(OAc)_2{\cdot}H_2O$ (20.0 mg or 28.3 mg, respectively). HOAc (250 μL) was added to dissolve chitosan completely. Fe NP@C and Co NP@C were prepared following the same procedure, but only using $Fe(OAc)_2$ (20.5 mg) or $Co(OAc)_2{\cdot}H_20$ (28.3 mg), respectively. After 2 h under magnetic string at room temperature, the solutions were dried by removing the water heating the solution at 70 °C overnight. The resulting samples were pyrolyzed under Ar flow (50 mL min^{-1}), increasing the temperature at a rate of 10 °C min^{-1} up to 900 °C with a holding time of 2 h.

Characterization techniques

Raman spectra were recorded at ambient temperature with 514 nm laser excitation on a Renishaw In Via Raman spectrometer equipped with a CCD detector. TEM images were recorded by using a Philips CM 300 FEG system with an operating voltage of 100 kV. XRD patterns were obtained by using a Philips X'Pert diffractometer and copper radiation ($Cu_{K\alpha}$ = 0.1541178 nm). Quantitative ICP–OES measurements were performed by using a 715-ES Varian apparatus. GC analysis was performed by using a Bruker 430-GC instrument equipped with a flame-ionization detector (FID) and a HP-5MS column (30 m × 0.25 mm × 0.25 mm) with a stationary phase constituted by crosslinked 5% phenylmethylsilicone. Products were isolated by column chromatography of the residue after removing DMA under reduced pressure using silica gel as stationary phase and CH_2Cl_2 as eluent.

Catalytic tests

Typically, the metal catalyst (1.6 mol%, total metal vs. substrate) was added to a reaction mixture of **1a** (0.1 mmol) in DMA (2 mL) inside a reinforced glass reactor. Then, the suspension was magnetically stirred while purging with Ar and heated at 110 °C with a preheated silicone bath. Once the reaction temperature was reached, the system was closed and pressurized with Ar (2.5 bar). Then, TBHP (5 M solution in decane) was introduced to the reaction mixture in two steps, 0.25 mmol at the starting time, and 0.15 mmol at 4 h reaction time. The temporal evolution of the reaction was followed by analyzing periodically known aliquots of solution taken with a syringe provided with a filter (0.2 μm) to remove the solid catalyst. The aliquots were immediately analyzed by GC. Indole was used as internal standard and yields were based on GC analysis of the reaction mixture containing weight amounts of indole as external standard. Experiments using $Fe(CO)_5$, $FeCl_2$ or $Fe(OAc)_3$ as homogeneous catalysts were conducted in the same conditions as indicated above with 5.3, 3.4, 6.5 μg for each of this catalyst, respectively, corresponding to 1.5 μg of Fe. The amounts were taken by weighing the amounts in mg dissolving in 1 mL of

DMA and taking 1 μL of the solution with a syringe. Formation of compound **3a** in yields below 5% was observed after 24 h.

Reuse experiment

Once the reaction was finished, the catalyst was recovered from the reaction mixture by filtration (Nylon filter, 0.2 μm), washed three times with DMA (3×10 mL) and dried in an oven (70 °C) overnight. Then, the catalyst was used again in the next C–N coupling reaction under the same conditions.

Accessibility tests

Portions of 50 mg of the as-synthesized samples (Fe NP@C, Fe-$Co_{0.86}$ NP@C or Co NP@C, respectively) were treated in 0.5 M HCl (15 mL) at room temperature under stirring for 14 h. Then, the samples were filtrated and the amounts of leached metals were determined by ICP–OES. Relative to the total metal content, 87.3% of total iron content in Fe NP@C and 85.5% of total iron content and 87.5% of total cobalt content in Fe–Co $NP_{0.86}$@C, and 88.4% of total cobalt content in Co NP@C were dissolved under these conditions. As it is well known, the acid leaching under diluted HCl at ambient temperature can only remove the accessible Fe and Co NPs embedded in the graphite shells. From these results, it seems that the Fe and Co NPs in the as-synthesized catalysts have similar metal accessibility.

Acknowledgements

Financial support by the Spanish Ministry of Economy and Competitiveness (Severo Ochoa and CTQ2015-69153-CO2-1) and Generalitat Valenciana (Prometeo 2013-014) is gratefully acknowledged. J.H. thanks the Chinese Scholarship Council for a doctoral fellowship at Valencia. A.D.M. thanks University Grants Commission, New Delhi, for the award of Assistant Professorship under its Faculty Recharge Program. A.D.M. also thanks the Department of Science and Technology, India, for the financial support through the Extra Mural Research funding (EMR/2016/006500).

Conflict of interest

The authors declare no conflict of interest.

Keywords: amides · carbon · iron · nanoparticles · radical reactions

[1] D. Astruc, F. Lu, J. R. Aranzaes, *Angew. Chem. Int. Ed.* **2005**, *44*, 7852–7872; *Angew. Chem.* **2005**, *117*, 8062–8083.
[2] M. Haruta, *CATTECH* **2002**, *6*, 102–115.
[3] R. Narayanan, M. A. El-Sayed, *J. Phys. Chem. B* **2005**, *109*, 12663–12676.
[4] Y. Mikami, A. Dhakshinamoorthy, M. Alvaro, H. Garcia, *Catal. Sci. Technol.* **2013**, *3*, 58–69.
[5] M. Haruta, *Catal. Today* **1997**, *36*, 153–166.
[6] M. Haruta, *Gold Bull.* **2004**, *37*, 27–36.
[7] R. Chinchilla, C. Najera, *Chem. Soc. Rev.* **2011**, *40*, 5084–5121.
[8] A. Dhakshinamoorthy, S. Navalon, M. Alvaro, H. Garcia, *ChemSusChem* **2012**, *5*, 46–64.
[9] V. Farina, *Adv. Synth. Catal.* **2004**, *346*, 1553–1582.
[10] R. J. White, R. Luque, V. L. Budarin, J. H. Clark, D. J. Macquarrie, *Chem. Soc. Rev.* **2009**, *38*, 481–494.
[11] M. Comotti, W. C. Li, B. Spliethoff, F. Schüth, *J. Am. Chem. Soc.* **2006**, *128*, 917–924.
[12] N. Lopez, T. V. W. Janssens, B. S. Clausen, Y. Xu, M. Mavrikakis, T. Bligaard, J. K. Nørskov, *J. Catal.* **2004**, *223*, 232–235.
[13] M. Okumura, S. Nakamura, S. Tsubota, T. Nakamura, M. Azuma, M. Haruta, *Catal. Lett.* **1998**, *51*, 53–58.
[14] S. Pisiewicz, D. Formenti, A.-E. Surkus, M.-M. Pohl, J. Radnik, K. Junge, C. Topf, S. Bachmann, M. Scalone, M. Beller, *ChemCatChem* **2016**, *8*, 129–134.
[15] F. A. Westerhaus, R. V. Jagadeesh, G. Wienhoefer, M.-M. Pohl, J. Radnik, A.-E. Surkus, J. Rabeah, K. Junge, H. Junge, M. Nielsen, A. Brückner, M. Beller, *Nat. Chem.* **2013**, *5*, 537–543.
[16] A. Banerjee, R. Gokhale, S. Bhatnagar, J. Jog, M. Bhardwaj, B. Lefez, B. Hannoyer, S. Ogale, *J. Mater. Chem.* **2012**, *22*, 19694–19699.
[17] J. A. Hu, H. L. Wang, Q. M. Gao, H. L. Guo, *Carbon* **2010**, *48*, 3599–3606.
[18] T. A. Wezendonk, Q. S. E. Warringa, V. P. Santos, A. Chojecki, M. Ruitenbeek, G. Meima, M. Makkee, F. Kapteijn, J. Gascon, *Farad. Discuss* **2016**, DOI: https://doi.org/10.1039/C6FD00198J.
[19] T. A. Wezendonk, V. P. Santos, M. A. Nasalevich, Q. S. E. Warringa, A. I. Dugulan, A. Chojecki, A. Koeken, M. Ruitenbeek, G. Meima, H. U. Islam, G. Sankar, M. Makkee, F. Kapteijn, J. Gascon, *ACS Catal.* **2016**, *6*, 3236–3247.
[20] B. An, K. Cheng, C. Wang, Y. Wang, W. Lin, *ACS Catal.* **2016**, *6*, 3610–3618.
[21] V. P. Santos, T. A. Wezendonk, J. J. D. Jaén, A. I. Dugulan, M. A. Nasalevich, H. U. Islam, A. Chojecki, S. Sartipi, X. Sun, A. A. Hakeem, A. C. J. Koeken, M. Ruitenbeek, T. Davidian, G. R. Meima, G. Sankar, F. Kapteijn, M. Makkee, J. Gascon, *Nat. Commun.* **2015**, *6*, 6451.
[22] K. P. De Jong, J. W. Geus, *Catal. Rev. Sci. Eng.* **2000**, *42*, 481–510.
[23] S. H. Joo, S. J. Choi, I. Oh, J. Kwak, Z. Liu, O. Terasaki, R. Ryoo, *Nature* **2001**, *412*, 169–172.
[24] P. Serp, M. Corrias, P. Kalck, *Appl. Catal. A* **2003**, *253*, 337–358.
[25] Z. Chen, D. Higgins, A. Yu, L. Zhang, J. Zhang, *Energy Environ. Sci.* **2011**, *4*, 3167–3192.
[26] B. D. Sherry, A. Fuerstner, *Acc. Chem. Res.* **2008**, *41*, 1500–1511.
[27] I. Thomé, A. Nijs, C. Bolm, *Chem. Soc. Rev.* **2012**, *41*, 979–987.
[28] G. Saidulu, R. A. Kumar, K. R. Reddy, *Tetrahedron Lett.* **2015**, *56*, 4200–4203.
[29] Q. Xia, W. Chen, *J. Org. Chem.* **2012**, *77*, 9366–9373.
[30] T. Truong, K. D. Nguyen, S. H. Doan, N. T. S. Phan, *Appl. Catal. A* **2016**, *510*, 27–33.
[31] F. Chen, C. Topf, J. Radnik, C. Kreyenschulte, H. Lund, M. Schneider, A. E. Surkus, L. He, K. Junge, M. Beller, *J. Am. Chem. Soc.* **2016**, *138*, 8781–8788.
[32] X. J. Cui, Y. H. Li, S. Bachmann, M. Scalone, A. E. Surkus, K. Junge, C. Topf, M. Beller, *J. Am. Chem. Soc.* **2016**, *138*, 457.
[33] L. He, F. Weniger, H. Neumann, M. Beller, *Angew. Chem. Int. Ed.* **2016**, *55*, 12582–12594; *Angew. Chem.* **2016**, *128*, 12770–12783.
[34] I. Ziccarelli, H. Neumann, C. Kreyenschulte, B. Gabriele, M. Beller, *Chem. Commun.* **2016**, *52*, 12729–12732.
[35] A. Primo, P. Atienzar, E. Sanchez, J. M. Delgado, H. Garcia, *Chem. Commun.* **2012**, *48*, 9254–9256.
[36] A. Primo, E. Sanchez, J. M. Delgado, H. Garcia, *Carbon* **2014**, *68*, 777–783.
[37] G. Abellán, M. Latorre-Sánchez, V. Fornés, A. Ribera, H. García, *Chem. Commun.* **2012**, *48*, 11416–11418.
[38] M. Latorre-Sanchez, P. Atienzar, G. Abellan, M. Puche, V. Fornes, A. Ribera, H. Garcia, *Carbon* **2012**, *50*, 518–525.
[39] E. Park, J. Q. Zhang, S. Thomson, O. Ostrovski, R. Howe, *Metall. Mater. Trans. B* **2001**, *32*, 839–845.
[40] S. Peng, C. Wang, J. Xie, S. Sun, *J. Am. Chem. Soc.* **2006**, *128*, 10676–10677.
[41] A. Primo, I. Esteve-Adell, J. F. Blandez, A. Dhakshinamoorthy, M. Alvaro, N. Candu, S. M. Coman, V. I. Parvulescu, H. Garcia, *Nat. Commun.* **2015**, *6*, 8561.
[42] A. Primo, I. Esteve-Adell, S. N. Coman, N. Candu, V. I. Parvulescu, H. Garcia, *Angew. Chem. Int. Ed.* **2016**, *55*, 607–612; *Angew. Chem.* **2016**, *128*, 617–622.
[43] D. Mateo, I. Esteve-Adell, J. Albero, J. F. Sánchez Royo, A. Primo, H. Garcia, *Nat. Commun.* **2016**, *7*, 11819.

[44] M. Buaki-Sogo, M. Serra, A. Primo, M. Alvaro, H. Garcia, *ChemCatChem* **2013**, *5*, 513 – 518.
[45] C. Lavorato, A. Primo, R. Molinari, H. Garcia, *ACS Catal.* **2014**, *4*, 497 – 504.
[46] S. L. Buchwald, C. Bolm, *Angew. Chem. Int. Ed.* **2009**, *48*, 5586 – 5587; *Angew. Chem.* **2009**, *121*, 5694 – 5695.

Manuscript received: March 10, 2017
Accepted manuscript online: March 27, 2017
Version of record online: July 11, 2017